nature astronomy

LETTERS

https://doi.org/10.1038/s41550-021-01516-8

Check for updates

A universal correlation between warm and hot gas in the stripped tails of cluster galaxies

Ming Sun[1]✉, Chong Ge[1]✉, Rongxin Luo[1]✉, Masafumi Yagi[2], Pavel Jáchym[3], Alessandro Boselli[4], Matteo Fossati[5,6], Paul E. J. Nulsen[7,8], Michitoshi Yoshida[9] and Giuseppe Gavazzi[5]

The impact of ram pressure stripping on galaxy evolution is well known (for example, ref. [1]). Recent multi-wavelength data have revealed many examples of galaxies undergoing stripping, often accompanied with multi-phase tails[2–13]. As energy transfer in the multi-phase medium is an outstanding question in astrophysics, galaxies in stripping are great objects to study. Despite the recent burst of observational evidence, the relationship between gas in different phases in the tails is poorly known. Here we report a strong linear correlation between the X-ray surface brightness and the Hα surface brightness of the diffuse gas in the stripped tails at ~10–40 kpc scales, with a slope of ~3.5. This discovery provides evidence for the mixing of the stripped interstellar medium with the hot intra-cluster medium as the origin of the multi-phase tails. The established relation in stripped tails, also in comparison with the probably related correlations in similar environments such as galactic winds and X-ray cool cores, provides an important test for models of energy transfer in the multi-phase gas. It also indicates the importance of the Hα data to study clumping and turbulence in the intra-cluster medium.

We have constructed the largest sample of ram pressure stripping (RPS) galaxies in nearby clusters with both deep Hα data (tracing warm gas with $T \approx 10^4$ K) from narrow-band imaging or MUSE integral-field spectrograph and deep X-ray data (tracing hot gas with $T \approx 10^7$ K) from Chandra or XMM-Newton (Table 1 and Supplementary Tables 1 and 2). All 17 galaxies have Hα tails detected by previous work and 12 of them have X-ray tails detected, including 6 new ones presented in this work. The tails are divided into 42 regions with sizes from 6.3 kpc^2 to 2.1×10^3 kpc^2, all beyond D_{25} (the isophotal level of 25 mag arcsec^{-2} in the B band) of the galaxy. The X-ray surface brightness (SB) in these regions, with point sources excluded, is measured. If undetected, 5σ upper limits for the X-ray emission are derived (for 8 regions in 7 tails). The X-ray bolometric fluxes and luminosities are also derived. Similarly, the Hα SB in these regions, with background sources and H II regions excluded, is also measured. As shown in Fig. 1, there is a strong correlation between the X-ray SB and the Hα SB in the tail regions. The correlation is well described by a simple linear relation of $SB_X/SB_{H\alpha} = 3.48 \pm 0.25$ (mean ± s.d., as also shown in the right panel of Fig. 1) and the intrinsic scatter of the correlation is small at ~10%. Our simple linear relation is also different from the previous correlation derived from one galaxy[14].

We can also examine individual Hα/X-ray tails. ESO 137-001 hosts the brightest Hα/X-ray tail[15,16]. We present a new Hα image of ESO 137-001, with new MUSE data to achieve complete coverage of its X-ray tail. As shown in Fig. 2 and Supplementary Figures 1 and 2, the general positional correlation between Hα and X-rays is very good. Both show double tails extending to at least 80 kpc from the galaxy. We are able to study the Hα–X-ray correlation in 14 tail regions of ESO 137-001. As is the case for every RPS tail, the study is limited by the X-ray data. Beyond ~15 kpc from the nucleus, the MUSE exposure is only 15–35 minutes per field, but sufficiently deep to probe the Hα emission at ~ kpc scales. By contrast, the Chandra exposure is 38.4 hours that covers the whole tail region, and the median area of tail regions is 136 kpc^2. On the other hand, it is unclear whether such a correlation still holds at ~ kpc scales, given the observed scatter at ~10–40 kpc scales. One upper limit for ESO 137-001 is around some Hα diffuse emission just beyond the primary X-ray tail (Fig. 2). Further X-ray extension beyond what is shown in Fig. 2 is indeed suggested from the Chandra temperature map[15]. We also show the X-ray and Hα images of other RPS tails in Supplementary Figs. 3–13. Generally good correlation between Hα and X-ray can be seen but the data quality (almost always for X-rays) does not allow for more detailed studies at smaller spatial scales. The X-ray properties of these tails are presented in the Supplementary Table 3.

We examined the correlation at similar region sizes of 300–440 kpc^2 and the results are the same (Supplementary Fig. 14). As the model with a constant X-ray/Hα ratio describes the data well, we also attempted to examine whether this constant depends on the cluster. The derived ratios are 3.1 ± 1.0, 2.5 ± 0.5, 2.8 ± 1.1, 3.7 ± 0.4 and 4.4 ± 0.7 for Virgo, A2626, A1367, A3627 and Coma respectively. Thus, while the current data may suggest a small cluster-to-cluster variation, more data are required to examine the trend with cluster mass or pressure of the intra-cluster medium (ICM). One factor to contribute to the scatter is the remaining H II regions, or recent star formation (SF). While the flux fraction of H II regions in our tail regions is typically very small (Supplementary Fig. 15), the X-ray/Hα ratio from SF is typically much smaller from our studies of galaxy regions (Supplementary Fig. 16). We also examined whether the X-ray/Hα ratio in the tail changes with the projected

[1]Department of Physics and Astronomy, University of Alabama in Huntsville, Huntsville, AL, USA. [2]National Astronomical Observatory of Japan, Mitaka, Tokyo, Japan. [3]Astronomical Institute of the Czech Academy of Sciences, Prague, Czech Republic. [4]Aix Marseille Université, CNRS, LAM (Laboratoire d' Astro physique de Marseille) UMR 7326, Marseille, France. [5]Dipartimento di Fisica G. Occhialini, Università degli Studi di Milano Bicocca, Milan, Italy. [6]INAF-Osservatorio Astronomico di Brera, Milan, Italy. [7]Center for Astrophysics, Harvard & Smithsonian, Cambridge, MA, USA. [8]ICRAR, University of Western Australia, Crawley, Western Australia, Australia. [9]Subaru Telescope, National Astronomical Observatory of Japan, Hilo, HI, USA. ✉e-mail: ms0071@uah.edu; gc0034@uah.edu; rl0055@uah.edu

Table 1 | The sample of the RPS galaxies in this work

Galaxy (cluster)	Redshift	L_{W1}[a]	SFR[b]	L_{FIR}[c]	r[d]	Number[e]
Unit		($10^9 L_\odot$)	($M_\odot\,yr^{-1}$)	($10^9 L_\odot$)	(kpc)	
NGC 4569 (Virgo)	-0.00078	0.74	1.3	$9.9^{+0.3}_{-0.8}$	477	5+1
NGC 4330 (Virgo)	0.00521	0.058	0.17	1.2±0.2	607	1+1
ESO 137-001 (A3627)	0.0154	0.49	0.97	5.2±0.1	172	14+2
ESO 137-002 (A3627)	0.0190	3.4	1.1	12.2±0.2	97	2+3
UGC 6697 (A1367)	0.0224	2.4	6.2	23±1	614	2+1
CGCG 097-073 (A1367)	0.0243	0.18	1.1	4.4±0.3	865	1+1
CGCG 097-079 (A1367)	0.0236	0.41	1.6	6.1±0.2	816	1+1
2MASX J11443212+2006238 (A1367)	0.0240	1.0	3.5	-	703	1+1
CGCG 097-092 (A1367)	0.0213	0.68	1.6	-	886	1+0
D100 (Coma)	0.0171	0.55	0.50	4.3±0.1	236	4+1
NGC 4848 (Coma)	0.0235	2.7	4.0	26.1±0.7	764	3+1
IC 4040 (Coma)	0.0262	1.9	2.9	27.9±0.5	406	1+1
GMP 2923 (Coma)	0.0289	0.083	0.10	-	346	1+0
GMP 3779 (Coma)	0.0185	0.82	1.2	6.9±0.2	554	1+1
GMP 3816 (Coma)	0.0315	0.91	1.5	9.8±0.2	362	1+1
GMP 4555 (Coma)	0.0277	0.60	0.81	5.7±0.2	656	1+1
IC 5337 (A2626)	0.0619	10	7.4	-	84	2+1

[a]The WISE band 1 (3.6 μm) luminosity as a proxy of the stellar mass. The Galactic extinction was corrected with the relation from ref. [46]. The typical errors are 2%–5%. [b]The star formation rate (SFR) derived from the Galaxy Evolution Explorer (GALEX) near-ultraviolet (NUV) flux density and the total far-infrared (FIR) luminosity from Hershel with the relation from ref. [47]. If the FIR luminosity is unavailable, the SFR is derived from the GALEX NUV flux density and the WISE 22 μm flux density with the relation from the same reference. The Kroupa IMF is assumed and the typical root mean squared scatter of the relation is ~23%. [c]the total FIR luminosity derived from the Herschel data [d]the projected distance of the galaxy to the cluster X-ray centre [e]the number of regions in the tail plus galaxy, respectively

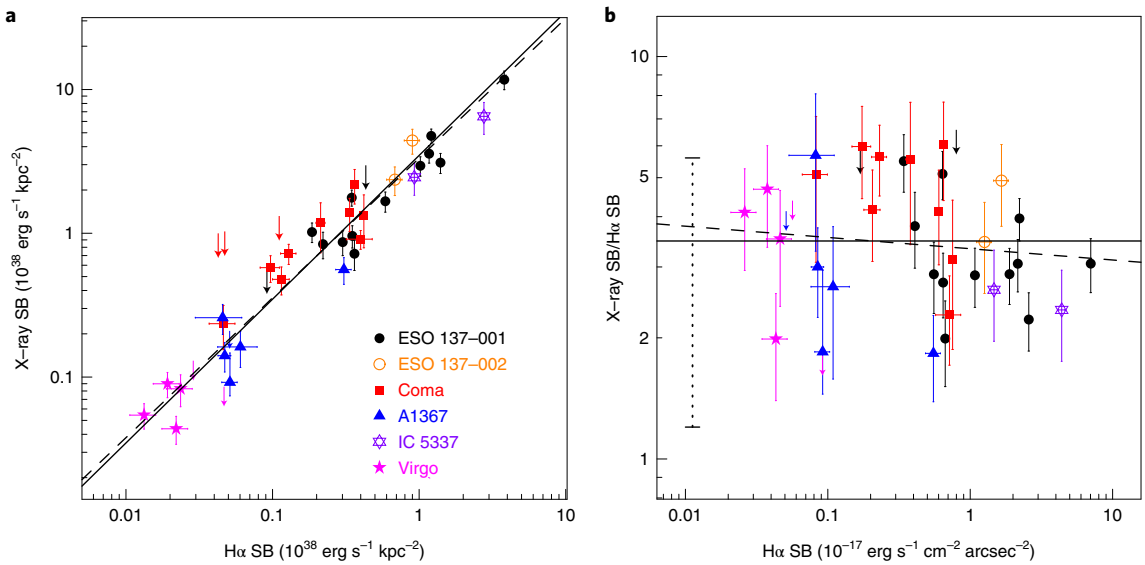

Fig. 1 | Hα–X-ray SB correlation for diffuse gas in stripped tails. X-ray luminosity and flux are bolometric. Errors for detections are 1σ. Upper limits (shown as arrows) are 5σ. **a**, The correlation shown as the luminosity SB. The black dashed line shows the best fit from the Bayesian method developed by ref. [48], with upper limits included (but excluding three upper limits in Coma as they are not constraining), $SB_X = (3.33 \pm 0.34) SB_{H\alpha}^{0.97 \pm 0.05}$. The black solid line shows the best fit with a slope of 1 from the same method, or $SB_X/SB_{H\alpha} = 3.48 \pm 0.25$. **b**, The correlation shown as the flux SB ratio versus the Hα flux SB. The solid and dashed lines are the same best fits as those in the left panel. In the ratio plot, three Coma tails with the ratio upper limits of higher than 10 are excluded as they are not constraining. The dotted line shows the ratios of 1.2–5.6 derived by ref. [18] for several regions in the galactic wind of NGC 253.

distance from the galaxy (Supplementary Fig. 17). The ratio probably increases at >60 kpc from the nucleus for one tail with the best X-ray data, but the results for other tails remain inconclusive. If mixing between the stripped interstellar medium (ISM) and ICM eventually depletes the stripped cold gas, the depletion is not observed from the ratio between the soft X-ray gas and the warm gas within ~60 kpc from the galaxy. However, it remains to be seen how the ratio of the hot (or warm) gas to the cold gas changes with the distance to the galaxy in stripped tails, ideally with the H I and CO data. We also examined the correlation between the X-ray/Hα

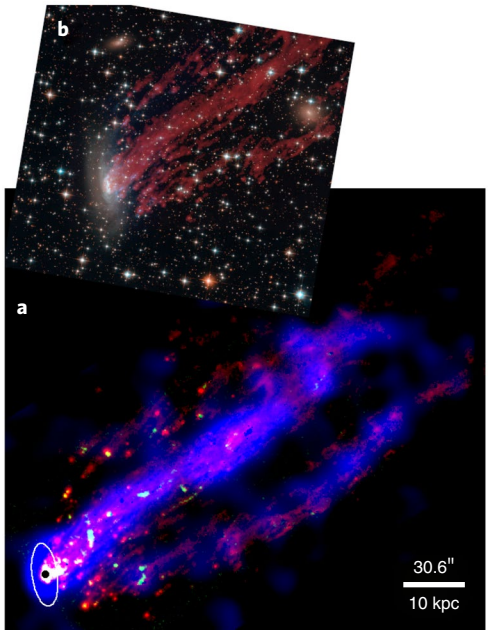

Fig. 2 | The Hα–X-ray correlation for ESO 137-001's tail with the brightest X-ray and Hα emission. a, The X-ray emission is shown in blue (0.6–2 keV from ref. [15]) and the Hα emission from this work is shown in red, while the CO (2–1) emission from ALMA[26] is shown in green. The nucleus of the galaxy is marked with a black dot and the white ellipse shows the half-light region of the galaxy from its Hubble Space Telescope F160W data. One can also see a very good correlation between the Hα and the X-ray diffuse emission in the tail. **b**, The Hubble Space Telescope composite image of the galaxy is also shown with the MUSE Hα in red. Credit: **b**, STScI.

ratio and the distance of the galaxy from the cluster centre, scaled by the virial radius or not, as well as the relative velocity of the galaxy to that of the cluster, scaled by the radial velocity dispersion of the cluster. No correlation was found.

Our results suggest that the formation of the X-ray tail is tightly related to the formation of the Hα tail, which in turn indicates a strong correlation between the hot gas and the warm gas. This is also strong evidence for mixing between the stripped ISM and the hot ICM, at spatial scales smaller than ~10 kpc, as good correlation has been established above this scale from the current data. The emissivity of both phases, all proportional to density squared, may have a similar dependence on the ambient pressure. We attempt a simple model to study this ratio and the results hinge on the detailed multi-phase gas distribution in small scales of the mixing layer (Supplementary Information). The multi-phase stripped tails have not been well studied in simulations and the correlation between different phases has not been examined in detail. Ref. [17] gave the total X-ray and Hα luminosities for stripped tails in three different simulation runs. The estimated X-ray/Hα ratio is 1.3–4.6 in these three runs, with the lowest ratio coming from the run with the lowest ambient pressure. More simulations are needed to better explore the Hα–X-ray correlation at different spatial scales and compare them with the observed relation. The evolution of this X-ray/Hα ratio is another interesting question to be addressed by simulations and observations in the future.

Stripped tails have become another kind of unique environment where a multi-phase medium and SF are present, similar to multi-phase galactic winds (for example, ref. [18]) and X-ray cool cores surrounding the brightest central galaxies in galaxy groups and clusters (for example, ref. [19]). Thus, it is natural to ask whether a similar relationship between X-ray and Hα exists in those two environments. However, such correlations in X-ray cool cores and galactic winds have not been studied in detail (Supplementary Information). The existing works on galactic winds of nearby starbursts have suggested a tight Hα/X-ray correlation with similar ratios to those found in stripped tails, while the X-ray/Hα ratios in X-ray cool cores are typically smaller. Future sample studies can explore the Hα–X-ray correlation in galactic winds and X-ray cool cores better.

In the stripped tails, the diffuse Hα emission (excluding emission related to H II regions or SF) probably originates from the turbulent mixing layer between the cold phase (molecular gas or/and atomic gas) and the hot ICM. Hydrodynamic instabilities and turbulence increase the contact surface between two phases and enhance mixing. We can consider the ratio between the turbulence eddy turnover timescale and the cooling timescale, $t_{\rm eddy}/t_{\rm cooling}$, the C-ratio (for example, ref. [20]) or the Damköhler number (for example, ref. [21]). This ratio may vary with locations in the multi-phase medium in stripped tails. In the ICM around the stripped tails, $t_{\rm cooling}$ is almost always longer than 10 Gyr. For a turbulence velocity of 100 km s^{-1} at a spatial scale of 10 kpc, $t_{\rm eddy}$ is 0.1 Gyr. Thus, the ratio should be much less than one for efficient mixing. When moving towards the stripped cold ISM, gas temperatures after mixing are lower and cooling can be much stronger to increase the $t_{\rm eddy}/t_{\rm cooling}$ ratio over 1, where inhomogeneous cooling results in a multi-phase medium. For the $T\approx10^{7}$ K gas in the stripped tails, $t_{\rm cooling}$ is typically 0.3–3 Gyr. For $T\approx10^{5-6}$ K gas, $t_{\rm cooling}$ should be much smaller. With an analogy to galactic winds, the stripped cold ISM clouds can grow via mixing under certain conditions (for example, refs. [22,23]), but can also fragment and even 'shatter' in the surrounding ICM, probably forming a complex distribution of small clumps resembling droplets (for example, ref. [24]). The magnetic field may also play an important role in mixing (for example, ref. [25]), as its existence is also implied by narrow Hα filaments observed in many tails of our sample.

Besides the Hα–X-ray (or warm gas–hot gas) correlation shown here, is there a tight correlation between other phases in stripped tails? The dominant mass component in stripped tails, at least at the early stage of stripping, is probably the molecular gas[10,12]. The cold gas in stripped tails, traced by H I and CO, should eventually be evaporated or cool to form stars, resulting in an increasing hot (or warm) gas to cold gas ratio. Ref. [12] explored the Hα–CO (or warm gas–cold gas) correlation but more CO detections from the stripped tails are required to explore the correlation better. Moreover, while compact molecular clouds have been revealed in the best-studied RPS tail of ESO 137-001 (ref. [26]) (also shown in Fig. 2), the same study also suggests most molecular gas is diffuse in the tail. Future studies may need to separate the compact/diffuse molecular components in the correlation studies.

Evaporating cold gas stripped from galaxies also contributes to the ICM clumping. The clumpiness of the ICM has been studied with X-ray observations, directly from, for example, SB fluctuation[27], or indirectly from, for example, cluster outskirts and scaling relations[28]. The ICM clumping can bias the measured X-ray properties of the cluster, for example, density, gas mass and pressure, which can further bias the resulting mass of the cluster[28,29]. Characterization of ICM clumping is important for current and next generation surveys in the X-ray and millimetre via the Sunyaev-Zel'dovich effect, as well as using clusters as precise cosmology probes. An important source of the ICM clumps is the stripped ISM, either by ram pressure or tidal force. When the stripped ISM evaporates in the ICM, it induces inhomogeneities. The tight correlation revealed by our studies suggests that at least some ICM clumps can be probed and even predicted by sensitive, wide-field Hα surveys (for example, ref. [30]). This discovery opens a new window to use Hα to trace hot gas structure in the ICM, including both the density fluctuations and the kinematic substructure.

Methods

We assume that the current value of the Hubble constant $H_0 = 70\,\mathrm{km\,s^{-1}\,Mpc^{-1}}$, the matter density parameter $\Omega_M = 0.3$ and the dark energy density parameter $\Omega_\Lambda = 0.7$. The distance to the Virgo cluster is 16.5 Mpc (ref. [31]) and the distance to the other clusters is derived from the assumed cosmological parameters. At the distance of the Virgo cluster, A3627, A1367 and Coma, 1″ corresponds to 80 pc, 327 pc, 445 pc and 466 pc, respectively. All X-ray spectra are fitted using the C-statistic and the quoted uncertainties are 1σ.

Chandra and XMM-Newton data processing. We processed the Chandra data with the Chandra Interactive Analysis of Observation (CIAO; version 4.12.1) and calibration database (CALDB; version 4.9.3), following the procedures in previous work[15,32].

We processed the XMM-Newton data using the Extended Source Analysis Software integrated into the XMM-Newton Science Analysis System (version 17.0.0), following the procedures in ref. [33]. Briefly, we reduce the raw event files from metal oxide semiconductor (MOS) and positive–negative junction (pn) CCDs using tasks emchain and epchain, respectively. The solar soft proton flares are filtered out with mos-filter and pn-filter to obtain clean event files.

For selected tail regions, the local background from regions adjacent to the tail regions is always used. The conversion from the count rate to the X-ray flux is derived from the spectral fit of the full tail region and is assumed to be the same for different tail regions. We use the AtomDB (version 3.0.9) database of atomic data and the solar abundance table from ref. [34]. We use the XSPEC apec model to fit the X-ray emission from tails. For the XMM-Newton data, the spectra from MOS/pn are fitted jointly. The galactic column density is modelled using tbabs, with values from the NHtot tool[35]. X-ray flux and luminosity shown are bolometric (0.01–100 keV).

Hα data processing. For six galaxies in the sample (ESO 137-001, UGC 6697, CGCG 097-073, CGCG 097-079, D100 and IC 5337), there is complete or partial coverage of their tails with MUSE. MUSE[36] is an optical integral-field spectrograph on the Very Large Telescope, which provides a 1′ × 1′ field of view with wavelength coverage from 4750 Å to 9350 Å in the nominal mode. For ESO 137-001, MUSE observations come from the European Southern Observatory (ESO) programmes 60.A-9349(A) (Science Verification), 60.A-9100(G) (Science Verification), 095.A-0512(A) (principal investigator or PI: M.S.) and 0104.A-0226(A) (PI: M.S.), with 12 pointings from 21 June 2014 to 17 March 2020 to cover the full tail. The total exposure time is 5 hours and 35 minutes, with the tail regions observed in 20.9–35 minutes and some galaxy regions observed in 90 minutes. The seeing is 0.57″–1.94″ with a median of 1.04″. The MUSE data effectively remove the Galactic stars and the resulting Hα image is much deeper than the narrow-band image by ref. [37]. This new mosaic also covers the tail much more completely than the old one published in refs. [16,38]. D100 was observed on 11 May 2019, under the ESO programme 0103.A-0684(A) (PI: P.J.), with a median seeing value of 1.12″. Only one field was observed with a total exposure time of 33 minutes to cover the galaxy and the front part of the tail. We also used the Hα flux maps measured with MUSE on three A1367 galaxies, UGC 6697, CGCG 097-073 and CGCG 097-079, under the ESO programmes 096.B-0019(A) and 098.B-0020(A) (PI: G.G.). The Hα flux map of UGC 6697 comes from ref. [39] and details of the observations can be found there. CGCG 097-073 was observed in three pointings, with 43 minutes on the galaxy and 38.85 minutes on 2 tail regions. CGCG 097-079 was observed in five pointings, with 43 minutes on the galaxy and 38.85 minutes on 4 tail regions. The observations of these 2 galaxies were taken from 12 February 2016 to 1 April 2017, with seeing of 0.35″–1.31″ (a median of 0.76″).

We used the MUSE pipeline (version 2.8.1; ref. [40]) to reduce the raw data. The MUSE pipeline was run with the ESO Recipe Execution Tool (EsoRex), which provides a standard procedure to reduce the individual exposures and combine them into a datacube. The additional sky subtraction was performed with the Zurich Atmosphere Purge software[41]. To combine the individual datacubes into the final mosaic, we adopted the CubeMosaic class implemented in the MUSE Python Data Analysis Framework (MPDAF) package[42]. For the final datacube mosaic, we adopted the public IDL software Kubeviz[38] to perform the spectral analysis. We first used the colour excess to correct the Galactic extinction, which was obtained from the recalibration[43] of the dust map of ref. [44] and adopted a galaxy extinction law from ref. [45] with the extinction coefficient $R_V = 3.1$. We also smoothed the datacube with a Gaussian kernel of 4 pixels (or 0.8″) for ESO 137-001 and 3 pixels (or 0.6″) for D100. We fitted the Gaussian profile to each emission line and obtained the flux. The spaxels with S/N < 3 and velocity error and velocity dispersion error >50 km s^{-1} are masked. The detailed MUSE results will be presented in future papers.

Other Hα data come from the narrow-band imaging observations as listed in Supplementary Table 2. [N II] emission is removed by assuming [N II] λ6584/Hα = 0.4 and [N II] λ6548/[N II] λ6584 = 1/3. Galactic extinction is corrected in all cases as stated above. Bright H II regions in the tail are masked for both the MUSE and narrow-band imaging data. The same criteria as used in ref. [38] are applied for the selection of H II regions. Specifically, SEXTRACTOR was run on Hα images. H II regions are selected as point-like sources (CLASS_STAR > 0.9) with a low ellipticity ($e < 0.2$). For diffuse Hα emission in tails, no correction on any intrinsic extinction was applied, for both narrow-band imaging data and the MUSE data. The correction on the stellar absorption was made on the galaxy for both MUSE and narrow-band imaging data. Such a correction has little effect on our results on tails since the stellar continuum beyond D_{25} is very weak.

Data availability

The X-ray and optical data that support the plots within this paper and other findings of this study are either publicly released (Chandra, XMM-Newton and Very Large Telescope/MUSE data) or published (narrow-band imaging data), as shown in Supplementary Table 2. The key results of this work (X-ray and Hα SB in tail regions) are also attached as an online table. Other results and reduced images of this work are available from the corresponding author M.S. upon reasonable request. Source data are provided with this paper.

Code availability

The software to reduce the X-ray and optical data in this work is publicly released. Upon request, the corresponding author M.S. will provide the code (Python and Wip) used to produce the figures.

Received: 1 March 2021; Accepted: 15 September 2021;
Published online: 13 December 2021

References

1. Boselli, A. & Gavazzi, G. Environmental effects on late-type galaxies in nearby clusters. *Publ. Astron. Soc. Pac.* **118**, 517–559 (2006).
2. Gavazzi, G. et al. 75 kiloparsec trails of ionized gas behind two irregular galaxies in A1367. *Astrophys. J.* **563**, L23–L26 (2001).
3. Sun, M. et al. A 70 kiloparsec X-ray tail in the cluster A3627. *Astrophys. J.* **637**, L81–L84 (2006).
4. Chung, A., van Gorkom, J. H., Kenney, J. D. P. & Vollmer, B. Virgo galaxies with long one-sided H I tails. *Astrophys. J.* **659**, L115–L119 (2007).
5. Yagi, M. et al. The remarkable 60 × 2 kpc optical filament associated with a poststarburst galaxy in the Coma cluster. *Astrophys. J.* **660**, 1209–1214 (2007).
6. Yoshida, M. et al. Strange filamentary structures ('fireballs') around a merger galaxy in the Coma cluster of galaxies. *Astrophys. J.* **688**, 918–930 (2008).
7. Yagi, M. et al. A dozen new galaxies caught in the act: gas stripping and extended emission line regions in the coma cluster. *Astron. J.* **140**, 1814–1829 (2010).
8. Smith, R. J. et al. Ultraviolet tails and trails in cluster galaxies: a sample of candidate gaseous stripping events in Coma. *Mon. Not. R. Astron. Soc.* **408**, 1417–1432 (2010).
9. Sivanandam, S., Rieke, M. J. & Rieke, G. H. A warm molecular hydrogen tail due to ram-pressure stripping of a cluster galaxy. *Astrophys. J.* **717**, 147–162 (2010).
10. Jáchym, P., Combes, F., Cortese, L., Sun, M. & Kenney, J. D. P. Abundant molecular gas and inefficient star formation in intracluster regions: ram pressure stripped tail of the Norma galaxy ESO137-001. *Astrophys. J.* **792**, 11 (2014).
11. Boselli, A. et al. Spectacular tails of ionized gas in the Virgo cluster galaxy NGC 4569. *Astron. Astrophys.* **587**, A68 (2016).
12. Jáchym, P. et al. Molecular gas dominated 50 kpc ram pressure stripped tail of the Coma galaxy D100. *Astrophys. J.* **839**, 114 (2017).
13. Poggianti, B. M. et al. GASP. I. Gas stripping phenomena in galaxies with MUSE. *Astrophys. J.* **844**, 48 (2017).
14. Poggianti, B. M. et al. GASP. XXIII. A jellyfish galaxy as an astrophysical laboratory of the baryonic cycle. *Astrophys. J.* **887**, 155 (2019).
15. Sun, M. et al. Spectacular X-ray tails, intracluster star formation, and ULXs in A3627. *Astrophys. J.* **708**, 946–964 (2010).
16. Fumagalli, M. et al. MUSE sneaks a peek at extreme ram-pressure stripping events. I. A kinematic study of the archetypal galaxy ESO137-001. *Mon. Not. R. Astron. Soc.* **445**, 4335–4344 (2014).
17. Tonnesen, S., Bryan, G. L. & Chen, R. How to light it up: simulating ram-pressure stripped X-ray bright tails. *Astrophys. J.* **731**, 98 (2011).
18. Strickland, D. K., Heckman, T. M., Weaver, K. A., Hoopes, C. G. & Dahlem, M. Chandra observations of NGC 253. II. On the origin of diffuse X-ray emission in the halos of starburst galaxies. *Astrophys. J.* **568**, 689–716 (2002).
19. Fabian, A. C. et al. The relationship between the optical Hα filaments and the X-ray emission in the core of the Perseus cluster. *Mon. Not. R. Astron. Soc.* **344**, L48–L52 (2003).
20. Gaspari, M. et al. Shaken snow globes: kinematic tracers of the multiphase condensation cascade in massive galaxies, groups, and clusters. *Astrophys. J.* **854**, 167 (2018).
21. Tan, B., Oh, S. P. & Gronke, M. Radiative mixing layers: insights from turbulent combustion. *Mon. Not. R. Astron. Soc.* **502**, 3179–3199 (2021).
22. Gronke, M. & Oh, S. P. The growth and entrainment of cold gas in a hot wind. *Mon. Not. R. Astron. Soc.* **480**, L111–L115 (2018).
23. Fielding, D. B., Ostriker, E. C., Bryan, G. L. & Jermyn, A. S. Multiphase gas and the fractal nature of radiative turbulent mixing layers. *Astrophys. J.* **894**, L24 (2020).

24. Gronke, M. & Oh, S. P. Is multiphase gas cloudy or misty? *Mon. Not. R. Astron. Soc.* **494**, L27–L31 (2020).
25. Sparre, M., Pfrommer, C. & Ehlert, K. Interaction of a cold cloud with a hot wind: the regimes of cloud growth and destruction and the impact of magnetic fields. *Mon. Not. R. Astron. Soc.* **499**, 4261–4281 (2020).
26. Jáchym, P. et al. ALMA unveils widespread molecular gas clumps in the ram pressure stripped tail of the norma jellyfish galaxy. *Astrophys. J.* **883**, 145 (2019).
27. Churazov, E. et al. X-ray surface brightness and gas density fluctuations in the Coma cluster. *Mon. Not. R. Astron. Soc.* **421**, 1123–1135 (2012).
28. Nagai, D. & Lau, E. T. Gas clumping in the outskirts of ΛCDM clusters. *Astrophys. J.* **731**, L10 (2011).
29. Vazza, F., Eckert, D., Simionescu, A., Brüggen, M. & Ettori, S. Properties of gas clumps and gas clumping factor in the intra-cluster medium. *Mon. Not. R. Astron. Soc.* **429**, 799–814 (2013).
30. Boselli, A. et al. A Virgo Environmental Survey Tracing Ionised Gas Emission (VESTIGE). I. Introduction to the survey. *Astron. Astrophys.* **614**, A56 (2018).
31. Mei, S. et al. The ACS Virgo cluster survey. XIII. SBF distance catalog and the three-dimensional structure of the Virgo cluster. *Astrophys. J.* **655**, 144–162 (2007).
32. Zhang, B. et al. The narrow X-ray tail and double Hα tails of ESO 137-002 in A3627. *Astrophys. J.* **777**, 122 (2013).
33. Ge, C. et al. X-ray scaling relations from a complete sample of the richest maxBCG clusters. *Mon. Not. R. Astron. Soc.* **484**, 1946–1971 (2019).
34. Asplund, M., Grevesse, N., Sauval, A. J. & Scott, P. The chemical composition of the sun. *Annu. Rev. Astron. Astrophys.* **47**, 481–522 (2009).
35. Willingale, R., Starling, R. L. C., Beardmore, A. P., Tanvir, N. R. & O'Brien, P. T. Calibration of X-ray absorption in our Galaxy. *Mon. Not. R. Astron. Soc.* **431**, 394–404 (2013).
36. Bacon, R. et al. The MUSE second-generation VLT instrument. In *Society of Photo-Optical Instrumentation Engineers Conference Series* Vol. 7735 (eds McLean, I. S. et al.) (SPIE, 2010).
37. Sun, M., Donahue, M. & Voit, G. M. Hα tail, intracluster H II regions, and star formation: ESO 137-001 in Abell 3627. *Astrophys. J.* **671**, 190–202 (2007).
38. Fossati, M. et al. MUSE sneaks a peek at extreme ram-pressure stripping events. II. The physical properties of the gas tail of ESO137-001. *Mon. Not. R. Astron. Soc.* **455**, 2028–2041 (2016).
39. Consolandi, G. et al. MUSE sneaks a peek at extreme ram-pressure events. III. Tomography of UGC 6697, a massive galaxy falling into Abell 1367. *Astron. Astrophys.* **606**, A83 (2017).
40. Weilbacher, P. M. et al. The data processing pipeline for the MUSE instrument. *Astron. Astrophys.* **641**, A28 (2020).
41. Soto, K. T., Lilly, S. J., Bacon, R., Richard, J. & Conseil, S. ZAP—enhanced PCA sky subtraction for integral field spectroscopy. *Mon. Not. R. Astron. Soc.* **458**, 3210–3220 (2016).
42. Bacon, R., Piqueras, L., Conseil, S., Richard, J. & Shepherd, M. MPDAF: MUSE Python Data Analysis Framework (2016).
43. Schlafly, E. F. & Finkbeiner, D. P. Measuring reddening with Sloan Digital Sky Survey stellar spectra and recalibrating SFD. *Astrophys. J.* **737**, 103 (2011).
44. Schlegel, D. J., Finkbeiner, D. P. & Davis, M. Maps of dust infrared emission for use in estimation of reddening and cosmic microwave background radiation foregrounds. *Astrophys. J.* **500**, 525–553 (1998).
45. Fitzpatrick, E. L. Correcting for the effects of interstellar extinction. *Publ. Astron. Soc. Pac.* **111**, 63–75 (1999).
46. Indebetouw, R. et al. The wavelength dependence of interstellar extinction from 1.25 to 8.0 μm using GLIMPSE data. *Astrophys. J.* **619**, 931–938 (2005).
47. Hao, C.-N. et al. Dust-corrected star formation rates of galaxies. II. Combinations of ultraviolet and infrared tracers. *Astrophys. J.* **741**, 124 (2011).
48. Kelly, B. C. Some aspects of measurement error in linear regression of astronomical data. *Astrophys. J.* **665**, 1489–1506 (2007).

Acknowledgements

M.S. thanks A. Fabian, Y. Li, S. Tonnesen and D. Wang for helpful discussions. We thank T. Edge and S. Laudari for work on the FIR data and the Hubble Space Telescope data. Support for this work was provided by the National Aeronautics and Space Administration (NASA) through Chandra Award Numbers GO6-17127X and GO6-17111X issued by the Chandra X-ray Center, which is operated by the Smithsonian Astrophysical Observatory for and on behalf of NASA under contract NAS8-03060. Support for this work was also provided by NASA grant 80NSSC19K0953 and the National Science Foundation grant 1714764. P.J. acknowledges support from the project EU-ARC.CZ (LM2018106) of the Ministry of Education, Youth and Sports of the Czech Republic. M.F. acknowledges support from the European Research Council (grant agreement no. 757535). This research has made use of data obtained from the Chandra Data Archive and the Chandra Source Catalog and software provided by the Chandra X-ray Center in the application packages CIAO. This research is also based on observations obtained with XMM-Newton, a European Space Agency science mission with instruments and contributions directly funded by European Space Agency Member States and NASA. This research is also based on observations collected at the European Southern Observatory under programmes 60.A-9349(A), 60.A-9100(G), 095.A-0512(A), 096.B-0019(A), 098.B-0020(A), 0103.A-0684(A) and 0104.A-0226(A). This research is based in part on data collected at Subaru Telescope, which is operated by the National Astronomical Observatory of Japan. We are honoured and grateful for the opportunity of observing the Universe from Maunakea, which has cultural, historical and natural significance in Hawaii.

Author contributions

M.S. initiated the research, led the Chandra and XMM-Newton proposals and the MUSE proposals on ESO 137-001, analysed the Chandra data, assisted with the MUSE data analysis and wrote the manuscript. C.G. analysed the XMM-Newton data and R.L. analysed the MUSE data from ESO 137-001 and D100. Both contributed to the writing of the manuscript. P.J. is the PI of the MUSE proposal on the Coma galaxies. G.G. is the PI of the MUSE proposal on the A1367 galaxies. M.F. analysed the MUSE data for A1367 galaxies. M.Y., M.F., G.G., A.B. and M.Y. provided the narrow-band Hα imaging data. All authors contribute to the discussion and interpretation of the results.

Competing interests

The authors declare no competing interests.

Additional information

Supplementary information The online version contains supplementary material available at https://doi.org/10.1038/s41550-021-01516-8.

Correspondence and requests for materials should be addressed to Ming Sun, Chong Ge or Rongxin Luo.

Peer review information *Nature Astronomy* thanks Florence Durret and the other, anonymous, reviewer(s) for their contribution to the peer review of this work.